JACS
JOURNAL OF THE AMERICAN CHEMICAL SOCIETY

ARTICLE

pubs.acs.org/JACS

His75−Asp97 Cluster in Green Proteorhodopsin

Franziska Hempelmann,[†] Soraya Hölper,[†] Mirka-Kristin Verhoefen,[‡] Andreas C. Woerner,[†] Thomas Köhler,[‡] Sarah-Anna Fiedler,[†] Nicole Pfleger,[†] Josef Wachtveitl,[*,‡] and Clemens Glaubitz[*,†]

[†]Institute of Biophysical Chemistry & Centre for Biomolecular Magnetic Resonance and [‡]Institute of Physical and Theoretical Chemistry, Goethe-University Frankfurt, Frankfurt, Germany

Supporting Information

ABSTRACT: The proteorhodopsin (PR) family found in bacteria near the ocean's surface consists of hundreds of PR variants color-tuned to their environment. PR contains a highly conserved single histidine at position 75, which is not found in most other retinal proteins. Using ^{13}C and ^{15}N MAS NMR, we were able to prove for green PR that His75 forms a pH-dependent H-bond with the primary proton acceptor Asp97, which explains its unusually high pK_a. The functional role of His75 has been studied using site-directed mutagenesis and time-resolved optical spectroscopy: Ultrafast vis-pump/vis-probe experiments on PR_{H75N} showed that the primary reaction dynamics is retained, while flash photolysis experiments revealed an accelerated photocycle. Our data show the formation of a pH-dependent His−Asp cluster which might be typical for eubacterial retinal proteins. Despite its stabilizing function, His75 was found to slow the photocycle in wild-type PR. This means that PR was not optimized by evolution for fast proton transfer, which raises questions about its true function in vivo.

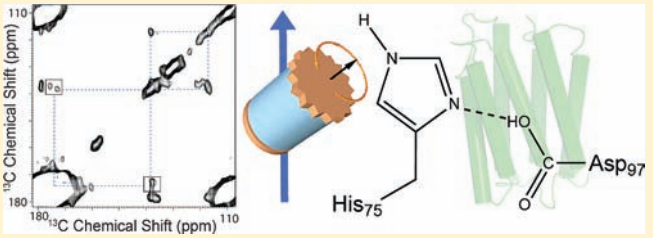

1. INTRODUCTION

Proteorhodopsins (PRs) are transmembrane retinal proteins, found in high abundance in bacteria in the photic zone of the oceans.[1,2] Especially the green-absorbing form (27 kDa, $\lambda_{max} \approx$ 520 nm) has been the focus of a number of studies. Green PR shares a 30% sequence identity with bacteriorhodopsin (BR). It contains the primary proton acceptor (Asp97), the proton donor (Glu108), the Schiff base (SB) linkage (Lys231), and counterions of the Schiff base (Arg94, Asp227).[3] The most striking difference from BR is the very high pK_a of the primary proton acceptor, the lack of an extracellular proton release group, and the occurrence of a highly conserved histidine at position 75 close to the photoactive site.[3,4] Low-resolution data obtained by atomic force and cryo electron microscopy show that PR assembles into pentameric or hexameric complexes.[5,6] Topology analysis, homology modeling, and solid-state NMR studies have confirmed that PR follows the typical seven transmembrane helix topology.[3,4,7,8] Solid-state NMR has also been used to probe the photoactive center of PR.[9,10]

It is well established that green PR works as a light-driven proton pump in vitro and in vivo when expressed in oocytes[3] or *Escherichia coli* cells.[11] PR undergoes a photocycle with a short turnover time of about 20 ms which contains K, L, M, N, and O intermediates.[12,13] The photocycle has been studied spectroscopically at different time scales in some detail.[12,14−21]

In this study, we have elucidated the role of His75. Homology modeling predicts its location in helix B close to the active site and near the primary proton acceptor Asp97 (Figure 1a).[4] The pK_a of histidine is in the physiological range. Therefore, its imidazole group is often involved in proton transfer reactions and could be of functional importance in PR. Using site-directed mutagenesis and time-resolved FTIR, Spudich and co-workers suggested a direct interaction between His75 and Asp97 and a direct involvement in proton transfer.[22] A possible interaction between both residues but no effect on the protonated Schiff base (pSB) was also reported by us.[10]

Here, we show by solid-state NMR that His75 forms a pH-dependent cluster with Asp97 through the formation of a H-bond. On the basis of our data, a mechanistic model which explains the stabilization of the high pK_a of the primary proton acceptor is presented. The functional role of His75 has been elucidated by a combination of site-directed mutagenesis and time-resolved optical spectroscopy and photocurrent measurements. Our results show that His75 is not essential for proton transfer and surprisingly slows the photocycle of wild-type (WT) PR. This result together with the high pK_a of Asp97 indicates that evolution has not optimized PR for fast proton transfer.

2. RESULTS

2.1. Site-Directed Mutagenesis and pH Titration. As described previously,[10] we have introduced the single-site mutations H75M, N, and W, which allow a direct assessment of the functional role of His75. A pH titration of the retinal optical absorption band of PR_{WT}, PR_{H75M}, PR_{H75N}, and PR_{H75W}

Received: December 22, 2010
Published: March 02, 2011

 © 2011 American Chemical Society

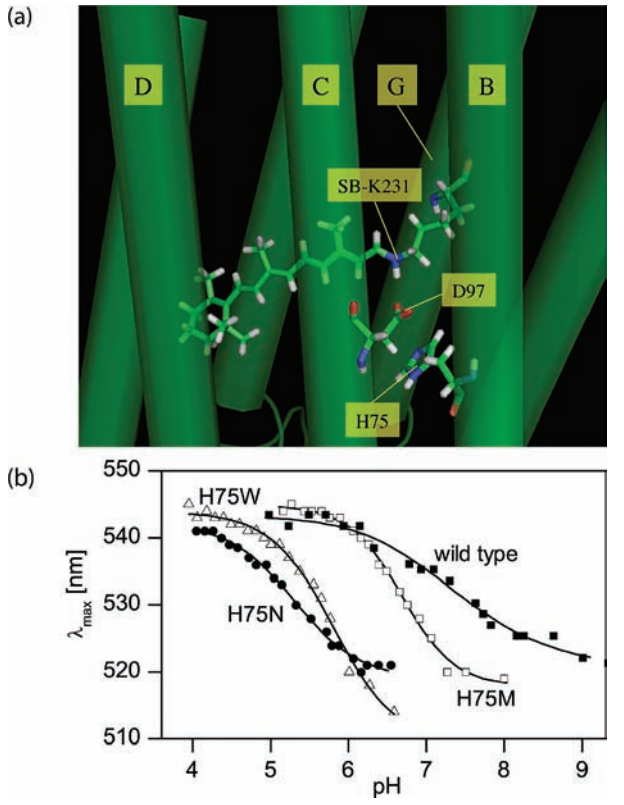

Figure 1. (a) A BR-based homology model of PR predicts a close proximity of His75 with Asp97. (b) A pH titration of the retinal optical absorption band of PR_{WT} and $PR_{H75M,N,W}$ solubilized in DDM shows that the pK_a of Asp97 is shifted from 7.5 (wild type, WT) to 6.7 (H75M), 5.8 (H75W), and 5.3 (H75N). This mutation-induced pK_a shift indicates a direct interaction between both residues.

solubilized in DDM is shown in Figure 1b. These mutations can be expected to disturb the interaction network of His75. A methionine is found in bacteriorhodopsin at this position. The pK_a of Asp97 is shifted from 7.5 (WT) to 6.7 (H75M), 5.8 (H75W), and 5.3 (H75N). This confirms previous data on reconstituted samples in which the same trend was observed.[10] These observations show that removal of His75 destabilizes the high pK_a of Asp97, indicating a direct interaction between both residues.

2.2. Solid-State NMR. Solid-state NMR has been used to probe close spatial proximity and a direct interaction between Asp97 and His75. Unfortunately, the PR wild-type construct used by us and others contains a His_6-tag for affinity purification.[3] Therefore, NMR signals of the single His75 residue will be obscured by signals from the His-tag. Attempts to remove the tag by proteolytic cleavage or to suppress its NMR signal by paramagnetic quenching were only partially successful. We have therefore used a PR construct without a His-tag which is purified by citrate precipitation.[23] Samples could be prepared in high purity (Figure S1, Supporting Information). Using this approach, we produced a sample in which His75 was ^{15}N-labeled at positions ND1, NE2, and N ([^{15}N-His]PR) and another sample in which His75 was fully ^{13}C labeled while all Asp residues were ^{13}C enriched at positions CG and C ([^{13}C-His-Asp]PR). Samples were reconstituted into lipid bilayers and subjected to CP-MAS (cross-polarization magic angle sample spinning) NMR experiments.

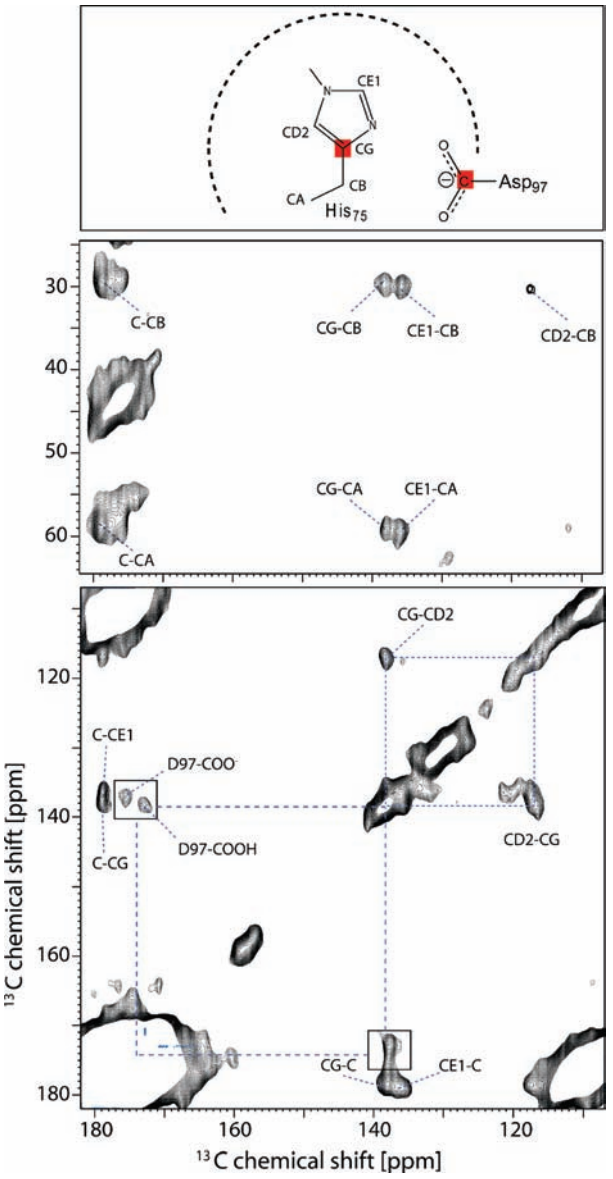

Figure 2. ^{13}C−^{13}C PDSD spectrum of [^{13}C-His-Asp]PR reconstituted into lipid bilayers at a pH close to the pK_a of Asp97. The C, CA, CB, CG, CD2, and CE1 resonances of His75 are found at 179.0, 58.9, 30.0, 138.0, 117.0, and 135.9 ppm. An additional inter-residue cross-peak between His75-CG and Asp97-CG-OOH at 172.7 and Asp97-CG-OO^- at 175.5 ppm is observed. A 800 ms mixing time was used.

2.2.1. ^{13}C CP-MAS NMR. A ^{13}C−^{13}C PDSD (proton-driven spin diffusion) spectrum of [^{13}C-His-Asp]PR at a pH close to the pK_a of Asp97 is shown in Figure 2. This experiment shows through-space ^{13}C−^{13}C correlations. All carbon signals of His75 are observable and well resolved. They could be unambiguously assigned on the basis of comparison between PDSD experiments using long and short mixing times, which enables differentiating between short-range and long-range contacts (Figure 2; Figure S2, Supporting Information). Especially resonances CD2 and CG are sensitive to the tautomeric forms His^{ND1} and His^{NE2} (see also Figure 7a). It was found that the ^{13}C chemical shift of CD2 is <122 ppm and that of CG >133 ppm for His^{NE2}, while for His^{ND1} ^{13}C chemical shifts of >122 ppm for CD2 and <133 ppm for CG have been described.[24,25] In our case, CG resonates at

dx.doi.org/10.1021/ja111116a |*J. Am. Chem. Soc.* 2011, 133, 4645–4654

138.0 ppm and CD2 at 117.0 ppm, which proves that His75 exists as the His^{NE2} tautomer in proteorhodopsin at this pH value. Furthermore, inter-residue contacts between His75-CG (138.0 ppm) and CG of an Asp at 175.5 and 172.7 ppm have been observed at very long mixing times, showing that these nuclei must be located within 6 Å from each other. The only Asp which is located close to His75 is Asp97 (see the Discussion below). Therefore, this inter-residue cross-peak can be assigned to a contact between His75-CG and CG of protonated and deprotonated Asp97.

2.2.2. ^{15}N CP-MAS NMR. The ^{15}N chemical shifts of both nitrogens in the imidazole ring are extremely sensitive to the His protonation state and to hydrogen bonds. We have therefore recorded ^{15}N CP-MAS spectra of [^{15}N-His]PR at different pH values which are shown in Figure 3a. Above pH 8, two resonances at 250 and 162.5 ppm are observed, which arise from the neutral form of His75 and can be assigned to ND1 and NE2, respectively. At pH 6, two peaks at 171 and 178 ppm are observed corresponding to ND1 and NE2 in the imidazole ion. In between, at pH 7, a superposition of both sets of signals is observed, with one additional ND1 resonance occurring at 239 ppm. This −11 ppm shift shows that ND1 is involved in a H-bond.[26−28] Deprotonated imidazole nitrogens are very difficult to observe because of their large chemical shift anisotropy and poor cross-polarization characteristics, which explains the small signal intensity of ND1 in Figure 3a. The ^{15}N resonances are relatively narrow, which means that only slow or no exchange of the imidazole ring occurs. Our experiments were carried out with a cys-less PR construct which has been purified by repetitive precipitation. To exclude that the ^{15}N results are caused by preparation artifacts, we have recorded ^{15}N spectra of wild-type [U-^{15}N]PR with a His-tag which has been purified conventionally. The same chemical shifts as shown in Figure 3 are observed for ND1 and NE2, but the spectra are obscured by the His-tag signal under acidic conditions (Figure S3, Supporting Information).

Since HD1 and HE2 protons are also sensitive reporters for the formation of H-bonds, we have recorded $^{15}N-^{1}H$ FSLG HETCOR (frequency-switched Lee−Goldburg heteronuclear correlation) spectra at two different pH values, above and below the pK_a of Asp97 (Figure 3b). This experiment creates through-space correlations between ^{15}N and ^{1}H nuclei via N−H dipole couplings; i.e., correlations between nitrogens ND1 and NE2 and directly bound protons HD1 and HE2 but also HB2/3 at the CB position and HE1 and HD2 at carbons CE1 and CD2 could be expected. At pH 6, cross-peaks between ND1 and NE2 with protons resonating at approximately 5 ppm are observed. On the basis of the statistical proton chemical shift boundaries[29] indicated in Figure 3b, it can be excluded that these signals are caused by directly bonded HD1 and HE2, although His75 is fully protonated. This could be due to fast exchange of these protons on the dipolar time scale. The observed cross-peaks most likely arise from the other nonexchangeable protons in His75 (HB2/3, HE1, HD1). Above pH 8, the sample contains both positively charged and neutral His75 populations. The cross-peak at 162.5 ppm/14 ppm belongs to NE2/HE2 of the neutral form. The weaker cross-peak pattern at approximately 6 ppm arises from the fully protonted His75 fraction as also observed at pH 6.

2.3. Time-Resolved Optical Spectroscopy. Our data presented above prove that a pH-dependent H-bond between His75 and Asp97 is formed. Replacing His75 with Met, Trp, or Asn destabilizes Asp97 (Figure 1b). The largest effect has been

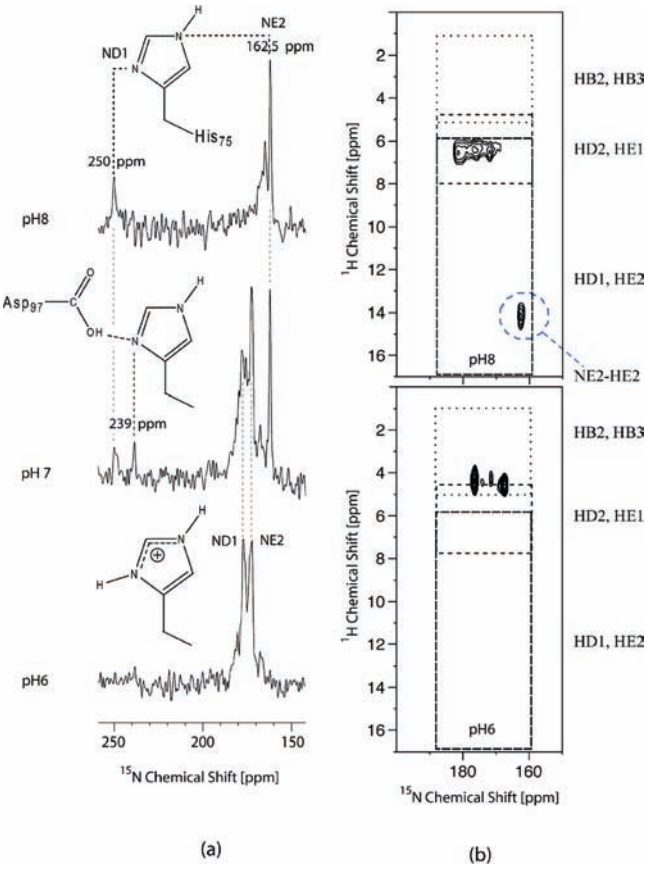

Figure 3. (a) ^{15}N CP-MAS NMR spectra of selectively labeled [^{15}N-His]-PR at different pH values. All signals arise from His75, which is the only His in PR. At pH 6 and below, two resonances for both protonated imidazole nitrogens ND1 and NE2 are observed at 178 and 171 ppm. At pH 7, three additional resonances at 250, 239, and 162.5 ppm are obtained. Above pH 8, His75 only shows two resonances at 250 and 162.5 ppm, which can be assigned to ND1 and NE2. The ND1 resonance at 239 ppm is evidence for the formation of a His−Asp H-bond (see the text for further details). (b) The HD1 and HE2 protons could not be detected at pH 6 and below in $^{1}H-^{15}N$ FSLG HETCOR experiments, but NE2 appears at 14 ppm above pH 8 when His75 is in its neutral form. Through-space correlations to other protons in His75 are seen under both conditions. The boxes indicate chemical shift range boundaries according to the BMRB database.[29]

observed for PR_{H75N}. We have therefore performed optical vis-pump/vis-probe and flash photolysis experiments on this mutant to elucidate the role of His75 for the light-induced retinal isomerization and for the subsequent photocycle steps of PR.

2.3.1. Vis-Pump/Vis-Probe Experiments on PR_{H75N}. Alterations of the primary reaction dynamics of PR_{H75N} have been measured by transient absorption spectroscopy in the visible spectral range. On the basis of the pH titration shown in Figure 1b, three pH values were selected at which Asp97 is deprotonated (pH 7.5), protonated (pH 4.2), or found close to its pK_a value (pH 5.6). The observed transient absorbance changes are shown as contour plots in Figure 4. Throughout the whole investigated time range, the spectral region between 450 and 650 nm is dominated by superimposed bands of the excited-state absorption (region A), the ground-state bleaching (region B), and the absorption of the photoproduct (region C). The signature of the stimulated emission is found above 650 nm (region D). The contour plots in Figure 4 show that

dx.doi.org/10.1021/ja111116a |J. Am. Chem. Soc. 2011, 133, 4645–4654

the observed spectral signatures between 450 and 650 nm are drastically pH dependent. At pH 4.2 and early delay times (<10 ps), the red wing of the excited-state absorption band (A) is fully superimposed by the ground-state depletion signal (B), while for pH 5.6 and 7.5, the excited-state absorption is the dominating feature. Due to contributions from the ground-state bleaching, the signal here splits into two parts, which are centered around 450 and 530 nm. Another striking pH-dependent difference is found at long delay times, where the positive signature of the photoproduct band (C) and the negative signal due to the depopulation of the *all-trans* retinal ground state (B) contribute. The spectra at a delay time of 1.0 ns therefore correspond to the $PR^{K}_{H75N}-PR_{H75N}$ difference spectrum. At pH 4.2, both bands nearly cancel each other, while high amplitudes are observed at pH 5.6 and 7.5. Similar observations have been made for PR_{WT}.[15,17,19] They most likely originate from a reduced spectral overlap of the ground state and K intermediate caused by the pH-dependent shift of the main retinal absorption band both in the wild type and in the mutants (Figure 1b).

The H75N mutation not only causes spectral changes but alters the reaction kinetics in a pH-dependent manner as well. The decay of the excited-state absorption band (A) is considerably elongated with decreasing pH. The same trend is observed in the region of stimulated emission (D). Since this band is not superimposed by any other signal, it is best suited to provide undisturbed insights into the S_1 decay. The exemplary transients (710 nm) at the bottom of Figure 4 show that stimulated emission occurs at pH 4.2 on a longer time scale than at pH 5.6 and 7.5. The transients also indicate that the excited state is not depopulated monoexponentially. Besides a depopulation time in the range of 10 ps, also a subpicosecond component is present. This fast deactivation pathway is more pronounced in the transients of the pH 7.5 sample, less important at pH 5.6, and nearly absent at pH 4.2. An analogous behavior with only some small deviations has been observed for PR_{H75M} (see the Supporting Information). A summary of the global fit analysis for PR_{H75N} and PR_{H75M} is given in Table S2, Supporting Information.

2.3.2. Flash Photolysis. To compare the photocycle kinetics of PR_{WT} with PR_{H75N}, flash photolysis experiments above, below, and close to the pK_a of Asp97 (Figure 1b) were carried out. The data are shown in Figure 5. The photocycle kinetics has been monitored via time courses at 410 nm (M intermediate), 510 nm (mainly ground state), and 590 nm (K and N/O intermediates). At a pH ≥ p$K_{a,D97}$, an absorption red-shifted from the PR ground state appears almost instantaneously after excitation in both samples. This signal spectrally resembles the photoproduct of the primary reaction and originates from the K intermediate. This contribution is seen in the transients at 590 and 510 nm and decreases on the microsecond time scale. The formation of a positive difference band is observed at 410 nm. This blue-shifted signal represents the M intermediate. The decay of this state is accompanied by an absorption increase red-shifted to the ground state (590 nm), which can be assigned to N and O intermediates.[3,12,20] The red-shifted intermediates decay on the millisecond time scale, thereby repopulating the ground state. At a pH < p$K_{a,D97}$, the amplitudes of the absorbance changes for both PR_{WT} and PR_{H75N} are generally smaller compared to those in the other two pH conditions. In both samples, very little or no accumulation of the M intermediate (410 nm) was found as described earlier for the wild type.[30] Only the K (and presumably

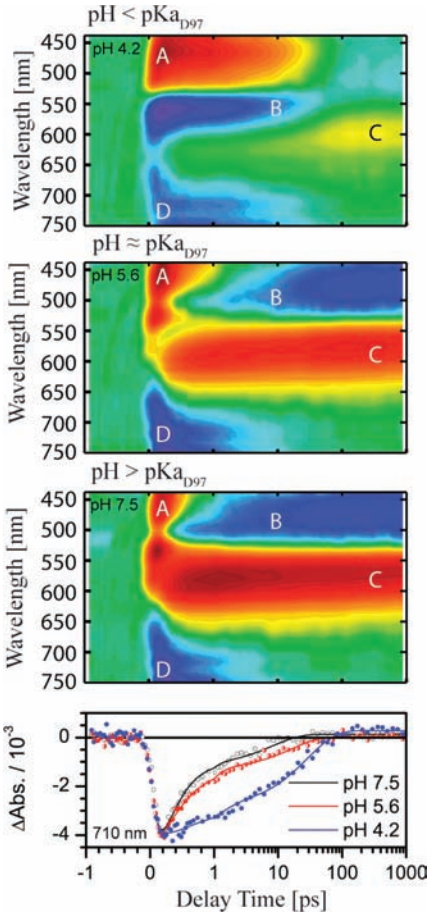

Figure 4. Transient absorbance changes of PR_{H75N} below, around, and above the pK_a of Asp97 (pH 4.2, 5.6, 7.5) after photoexcitation at 520 nm. The main contributions arise from the excited-state absorption (A), ground-state bleaching (B), absorption of the photoproduct PR^{K}_{H75N} (C), and stimulated emission (D). The amplitudes are color coded: red, positive aborbance changes; green, zero absorbance changes; blue, negative absorbance changes. The time axis is linear in the range from −1 to +1 ps and logarithmic for longer delay times. At the bottom trace, the pH-dependent transient absorbance changes for a probing wavelength in the region of the stimulated emission (710 nm) are compared.

also the L) state (510 nm) and late red-shifted intermediates (590 nm) are present to some extent.

Our data show that the photocycles of PR_{WT} and PR_{H75N} show the same basic features, but photocycle transitions and the turnover rate of PR_{H75N} are much faster. These differences are most prominent at pH ≥ p$K_{a,D97}$ and are less pronounced in the case of pH < p$K_{a,D97}$. We have analyzed both data sets by a rate model with four exponential terms, except for PR_{WT} at pH ≥ p$K_{a,D97}$, where five terms were needed. The results are shown in Table S3, Supporting Information. All time constants at the three pH values were found to be much shorter for PR_{H75N} compared to PR_{WT}. For example, the PR ground-state recovery described by two decay time constants, is accelerated from 44 and 210 ms for PR_{WT} to 6.1 and 56 ms for PR_{H75N} at pH > p$K_{a,D97}$. The M intermediate decays 5 times faster.

2.4. Photocurrent Measurements Using Black Lipid Membrane (BLM) Experiments. Photocurrent measurements have been carried out to verify whether PR is still able to transfer protons across the membrane after replacing His75. Upon continuous illumination with yellow light, characteristic photocurrents

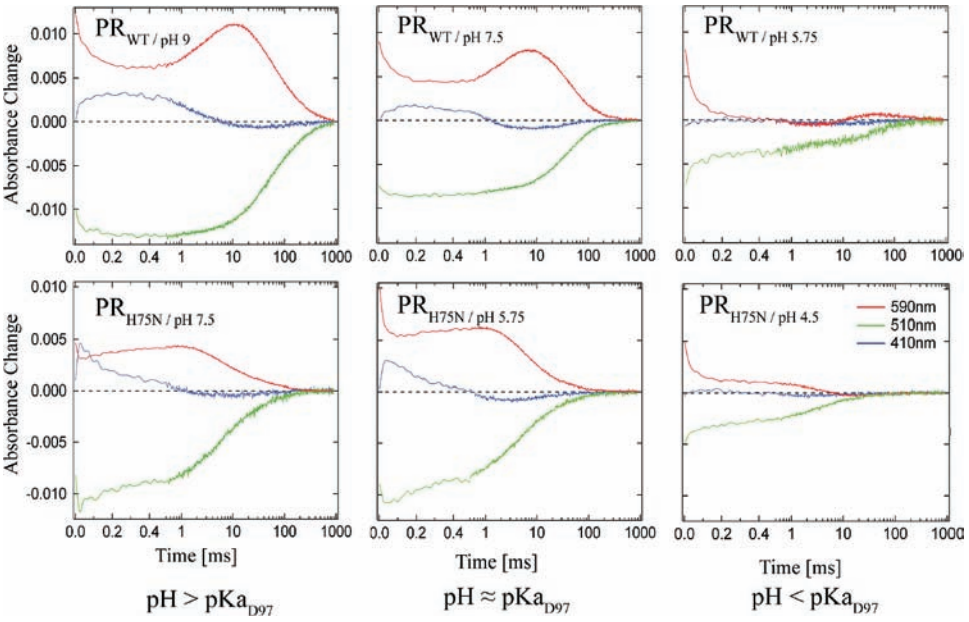

Figure 5. Laser flash induced time-dependent absorbance changes of solubilized PR_{WT} and PR_{H75N} mutant below, around, and above the pK_a of Asp97. All data sets are scaled to equal values of excitation pulse photon irradiance and protein concentrations. The mutant shows a spectral behavior similar to that of the wild type, but is significantly faster (see Table S3, Supporting Information).

mediated by PR_{WT} have been observed which are comparable to those reported before[3] (Figure 6). A very similar characteristic is obtained for PR_{H75N} (Figure 6) and PR_{H75M} (Figure S8, Supporting Information). These data show that these mutants are able to mediate net proton transfer with the same photocurrent size and direction as PR_{WT}.

3. DISCUSSION

3.1. Solid-State NMR. The $^{13}C-^{13}C$ spin diffusion data shown in Figure 2 reveal an inter-residue contact between CG of His75 and CG of an Asp. Although isotope labeling of Asp is not very efficient, other residue types can be excluded: Approximately 35% of added 1,4-$^{13}C_2$-Asp will scramble into Asn, Lys, Thr, Ile, and Met.[31,32] The CG carboxyl group in Asp will become a CG methylene group in those residues with a very different chemical shift (between 20 and 40 ppm). Therefore, potential cross-peaks between CG of His75 and CG of those scrambling products would occur in very different regions of the spectrum and would not contribute to the assigned Asp cross-peak. The reduced labeling efficiency of those scrambling products and their location in the PR homology model exclude correlation with His75. Therefore, the observed inter-residue contact can be assigned to a CG-His−CG-Asp correlation. The only aspartates close to His75 according to the PR homology model are Asp97 and Asp227.[4] The PR model predicts a His75-CG−Asp97-CG distance of 3.5 Å and for His75-CG−Asp227-CG a value of 7.8 Å. Furthermore, Shi et al. have reported ^{13}C chemical shifts of 175.4 ppm for Asp97 and 178.1 ppm for Asp227.[8] The corresponding value for Asp85 in BR is found at 173.7 ppm.[33] We have observed two signals at 173.5 and 175.5 ppm, which can be assigned to COOH and COO^- in Asp97. We can therefore conclude that the side chains of His75 and Asp97 are oriented to each other. A correlation with CG of Asp227 has not been observed. Neutralization of Asp227 by a D227N mutation shifts λ_{max} and results in a small decrease of the pK_a of Asp97

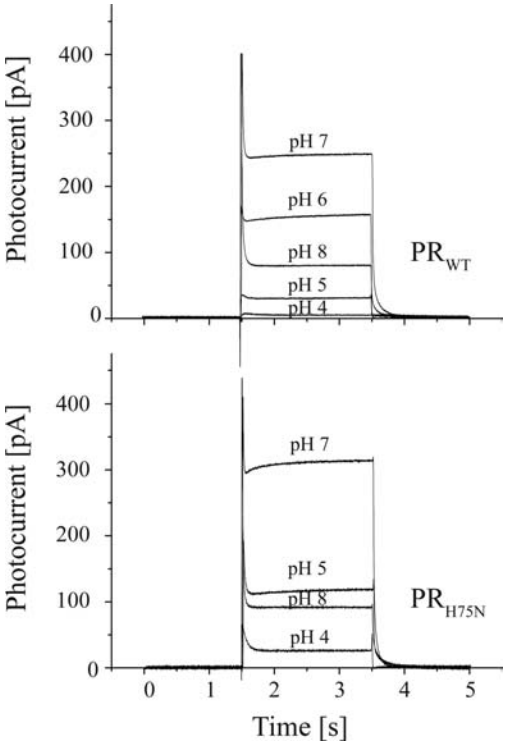

Figure 6. Stationary photocurrents of reconstituted PR_{WT} and PR_{H75N} in BLM experiments under full illumination with yellow light. Despite replacing His75, net transport of protons similar to that of wild-type PR is observed (see the Supporting Information for further details).

(Figure S5, Supporting Information), which could be caused by their close spatial proximity. Asp227 had been found to influence the isomerization of the retinal.[16] A more complex interaction pattern involving His75 with both Asp97 and Asp227, which form together the counterion complex, could be envisaged, but our data only support a direct contact between His75 and Asp97.

dx.doi.org/10.1021/ja111116a |J. Am. Chem. Soc. 2011, 133, 4645–4654

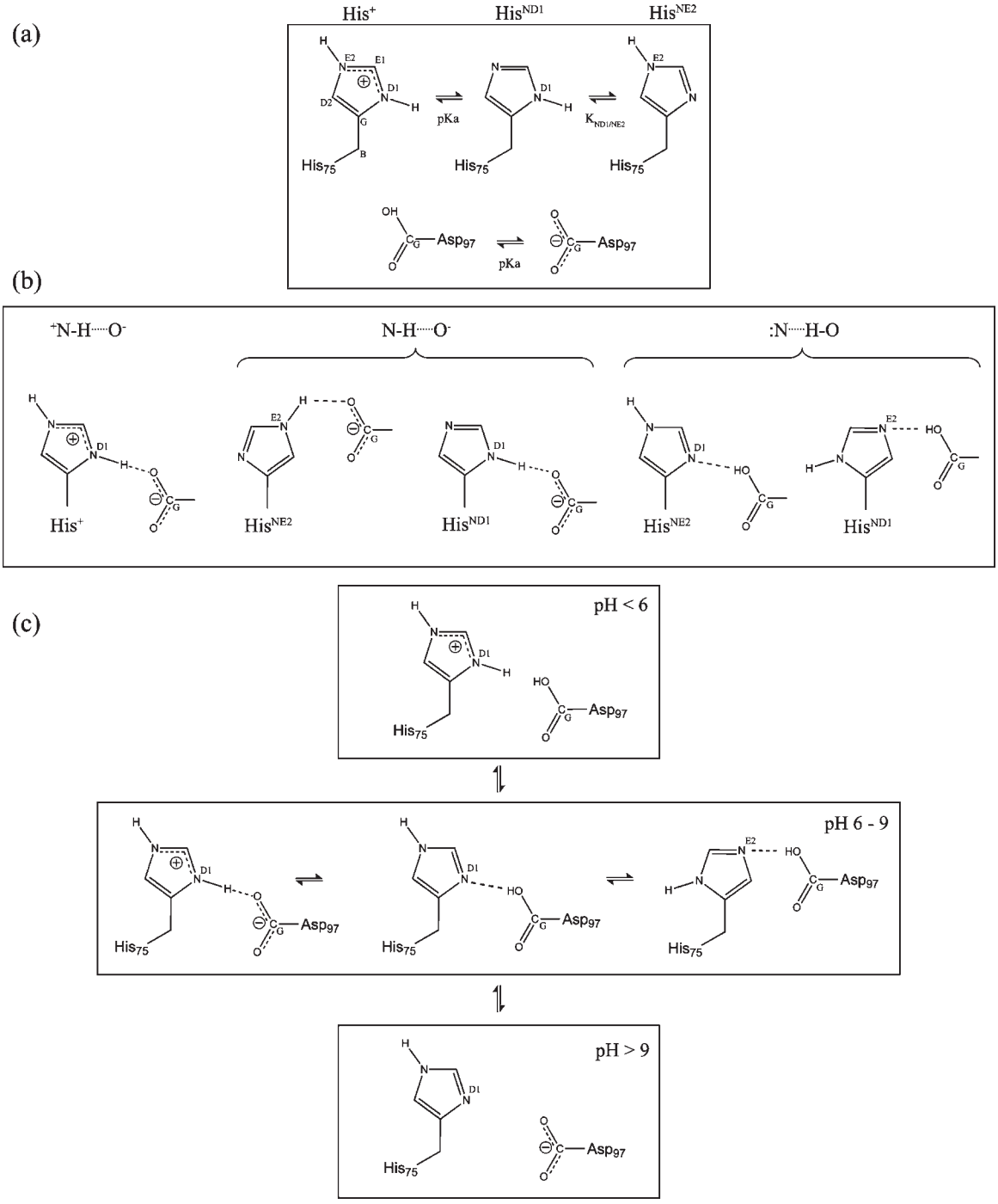

Figure 7. Different states in which His75 and Asp97 in PR could exist (a). For free His, $K_{ND1/NE2}$ is approximately 4.0. Five different types of H-bonds could occur between His75 and Asp97 (b), but only the type {:N···H−O} could stabilize the high-pK_a Asp97. Our data give rise to the following model for the formation of a pH-dependent His−Asp cluster in PR (c): Below pH 6, both residues are protonated. In the pH range between 6 and 9, an equilibrium among His^{+}, His^{ND1}, and His^{NE2} exists. Our data show that His^{NE2} is the dominating population which forms a {:N···H−O} bond between His75-ND1 and the carboxyl group of Asp97. This form is energetically favorable over {$^{+}$N−H···O^{-}},[35] explaining the unusually high pK_a of Asp97. Above pH 9, both residues are deprotonated.

This is also supported by the ^{15}N spectra of PR_{D227N}, which show the same H-bonding signal at 239 ppm as seen for PR_{WT} (see Figure S4, Supporting Information). Such a signal would not be expected if the H-bond from His75 involves Asp227.

Above its pK_a, free His exists in an equilibrium between the His^{ND1} and His^{NE2} tautomers (Figure 7a), which is shifted 4-fold toward His^{NE2}.[34] Therefore, His^{ND1} is found much less often in proteins. It only occurs in cases of His involved in structural interactions which stabilize His^{ND1} over His^{NE2}, when this His is pH invariant, shielded from the solvent, or strongly H-bonded. The His^{ND1} form is found, for example, in the active site of serine proteases, where a H-bond between ND1-H and the adjacent carboxylate group of the catalytic triad residue stabilizes this tautomer.[26] In the case of PR, the ^{13}C chemical shifts of CG and

dx.doi.org/10.1021/ja111116a |J. Am. Chem. Soc. 2011, 133, 4645–4654

CD2 in His75 reveal that it is a His^{NE2} tautomer, while His^{ND1} has not been observed. This means that His75 does not experience any stabilizing interaction in PR, which shifts the tautomerization equilibrium away from His^{NE2}. This is in line with our ^{15}N spectra (Figure 3a), which show that His75 fully responds to pH changes and must have a pK_a around 7, which is just slightly higher than for free His.

To stabilize the protonation state of the carboxyl group of Asp97 through His75, a H-bond needs to be formed. Our data clearly show that indeed CG of His75 and CG of Asp97 are within a range which would allow a H-bond between both side chains (Figure 2, top). The five possibilities for the coupling between His and Asp are shown in Figure 7b: (i) Nitrogens in the imidazole ion could couple to Asp97 via $\{^{+}N-H\cdots O^{-}\}$, while in the neutral species (ii) NE2 of His^{NE2} or ND1 of His^{ND1} could form $\{N-H\cdots O^{-}\}$, and (iii) ND1 of His^{NE2} or NE2 of His^{ND1} could form $\{:N\cdots H-O\}$.

To differentiate these three cases, all possible interactions of the imidazole ring need to be dissected. This is usually a difficult task due to the tautomerization of the neutral His species and because of different signals arising from protonated nitrogens in the charged and in the neutral species of His. All of these forms could coexist. Fortunately, our ^{13}C data have allowed the identification of His^{NE2} as the dominating form of neutral His75, and ^{15}N data show distinct differences among $^{+}N-H$, N−H, and :N (Figure 3a).

(i) Formation of $\{^{+}N-H\cdots O^{-}\}$: The observed ^{15}N chemical shifts at 171 and 178 ppm are probably too small for a H-bonded species.[26] Furthermore, the HD1 and HE2 protons have not been observed in $^{15}N-^{1}H$ FSLG HETCOR experiments (Figure 3b). In this experiment, protons are detected through a cross-polarization step via ^{15}N. The transfer efficiency depends on the $^{1}H-^{15}N$ through-space dipolar couplings as well as on the rotating frame spin−lattice relaxation time ($T_{1\rho}$). Both parameters could be affected by side chain mobility or fast proton exchange with the environment. If both protons are able to exchange on the relevant time scale, then they are most likely not involved in strong H-bond interactions at this pH. Simple side chain flexibility would also cause a reduction in ^{15}N cross-polarization efficiency, which has not been observed. In addition, this H-bond would not stabilize the protonation state of Asp97 as the proton would reside at NE2. Therefore, such a bond can be excluded as a main factor for the formation of a His−Asp cluster in PR.

(ii) Formation of $\{N-H\cdots O^{-}\}$: The ^{15}N chemical shift of NE2-H occurs shifted by approximately −10 ppm compared to that of $^{+}$NE2-H, which is in the expected range. The ^{1}H chemical shift of HE2 found at 14.5 ppm could indicate a H-bond, but this should also be reflected in a larger ^{15}N chemical shift for NE2 than observed. This is also supported by control experiments on PR_{D97N} (Figure S4, Supporting Information). The NE2 chemical shift changes by +4.5 ppm upon introduction of the D97N mutation. A potential H-bond between His75 and Asp97 would have been destroyed by this mutation, resulting in a larger chemical shift difference in the opposite direction.[26] Therefore, the formation of a $\{N-H\cdots O^{-}\}$ between His75 and Asp97 can be excluded and could not contribute to the stabilization of Asp97. Contributions from His^{ND1} can be neglected.

(iii) Formation of $\{:N\cdots H-O\}$: Our data show that His^{NE2} is the dominating form of His75. The formation of this H-bond would therefore cause a stronger shielding of the ND1 resonance in His75; i.e., a decrease of its chemical shift by approximately 10 ppm would be expected.[26] Here, we have been able to observe such a shift by −11 ppm for ND1 at pH 7 (Figures 3a; Figure S2, Supporting Information). This clearly shows the existence of such a H-bond and proves that it is actually ND1 stabilizing the protonation state of Asp97 via a His75-ND1···H-OD1-Asp97 H-bond. The spectrum in Figure 3a also shows that, at this pH, ground-state PR exists in an equilibrium between at least three different species: His75 in its neutral form, in its positively charged form, and in a H-bonded form with Asp97.

Our data demonstrate that the His75 and Asp97 side chains are oriented to each other and form a pH-dependent H-bond (Figures 2 and 3). Our findings are summarized in Figure 7c: (i) Below pH 6, both His75 and Asp97 are fully protonated. (ii) Above pH 8, His75 is in its neutral form while Asp97 is fully deprotonated. (iii) Between pH 6 and pH 8, an equilibrium between the charged and the neutral forms (His^{ND1}, His^{NE2}) of His75 is observed, both of which could be involved in couplings with Asp97. However, our data show that the H-bonded His^{NE2} species is the one to which the equilibrium is shifted. Quantum chemical calculations have shown that, in such H-bonded His−Asp pairs with a shared proton, the N···HO form is energetically favorable over the NH···O variant.[35] Therefore, our results explain unambiguously how the unusually high pK_a of Asp97 is stabilized. However, this H-bond formation is probably not the sole stabilization factor. If it was, all single-point mutations of position 75 which prevent the formation of such a H-bond should have the same destabilization effect, which is not the case (Figure 1b). Probably, the shielded location of Asp97 within the protein in the membrane raises its pK_a, which is further enhanced by His75. In addition, other residues could also have small additional stabilization effects.

3.2. Time-Resolved Optical Spectroscopy and BLM Experiments. Our solid-state NMR data show that His75 is essential for stabilizing the protonation state of the primary proton acceptor Asp97 in the ground state of PR. To elucidate the functional role of His75 for the primary reaction and photocycle dynamics, we have used time-resolved optical spectroscopy on PR_{WT} and PR_{H75N}. This mutant replaces the imidazole group with a nonprotonatable side chain and strongly destabilizes the pK_a of Asp97 (Figure 1b).

Using vis-pump/vis-probe spectroscopy, we have first probed the effect of this single-point mutation onto the primary reaction dynamics within the first 1000 ps upon light activation. We found that the pH-dependent isomerization dynamics of PR_{WT}, PR_{H75N}, and PR_{H75M} strongly resemble each other. Their time constants (Table S2, Supporting Information) mainly match the values for PR_{WT}.[17] After photoexcitation an ultrafast dynamics in the range of 100 fs is observed (τ_1). For the presented measurements this time constant is in the range of the time resolution, but referring to former papers on PR[17] and other retinal proteins,[36,37] one is nevertheless likely to assume that this time constant reflects an ultrafast wave packet motion out of the Franck−Condon region. For BR it is widely accepted that this movement is an in-plane stretching motion of the conjugated carbon chain, which is followed by a torsional motion around the $C_{13}-C_{14}$ double bond.[38] The reaction continues with a biexponential decay (τ_2, τ_3) of the excited-state population. This has been explained by a bifurcated excited-state deactivation pathway, in which two channels lead to the ground-state potential energy surface.[15,17] One may assume that the population of the faster reaction channel directly proceeds via a conical intersection to the ground state as has been shown for BR.[38] The slower

reaction pathway is discussed to include a small energetic barrier, which has to be overcome first.[15,17]

As previously observed for PR_{WT}[15,17,19] and PR_{D97N},[18,39] also PR_{H75N} and PR_{H75M} show two different variations on the biphasic deactivation pathway with varying pH: (i) The overall S1 depopulation kinetics is faster at pH > $pK_{a,D97}$ compared to pH < $pK_{a,D97}$. (ii) The amplitudes of the time constants (τ_2, τ_3) associated with the S1 decay change with pH, as shown in the decay-associated spectra (DAS) in Figures S6 and S7, Supporting Information. This can be interpreted in the the following way: the fast deactivation pathway is the dominating channel for a sample with a deprotonated counterion complex, whereas the slower reaction pathway plays the major role in samples with a protonated Asp97.

From the similarities among PR_{WT}, PR_{H75N}, and PR_{H75M}, it can be concluded that most electrostatic and steric properties as well as the H-bonding network in the vicinity of the retinal are well preserved. These results nicely fit our previous solid-state NMR studies, in which we showed that the direct Schiff base environment is not perturbed by these mutations (Figure S4, Supporting Information),[10] while a direct interaction between His75 and Asp97 is shown here. The small deviations in the primary reaction kinetics of PR_{H75M} compared to PR_{H75N} indicate a smaller pH dependence. The longest time constant τ_3 is slightly higher than for PR_{WT} and PR_{H75N}. One reason could be that the Met residue introduces a higher hydrophobicity in the environment of Asp97, resulting mainly in different electrostatic properties of the retinal binding pocket and therefore altered isomerization rates and less effect on the pK_a of the counterion complex. Our picosecond data on PR_{H75N} thus show unambiguously that the pK_a of the primary H^+-donor and not the absolute pH value is the main determinant for the primary reaction rate.

The H75N flash induced kinetics show clear evidence for the existence of K, M, and late red-shifted intermediates. In qualitative terms, the photocycle is very similar to that of PR_{WT}, but its pH-dependent characteristics are shifted according to the lower pK_a of Asp97. Photocurrent measurements using black lipid membranes provide clear evidence for active proton transfer by PR_{H75N} and PR_{H75M} (Figure 6; Figure S8, Supporting Information). Spudich and co-workers introduced single-point mutations at position 75 using a neutral (Ala), an acidic (Glu), and a basic (Arg) residue.[22] Using time-resolved FTIR, they showed that these mutants undergo a photocycle, but evidence for light-induced charge transfer in PR_{H75R} was not found. A striking effect of the H75N mutation is the significant acceleration of the photocycle under all three pH conditions. Using time-resolved FTIR, Spudich and co-workers also observed a significant faster return to the initial state of the H75A and H75E mutants compared to the PR_{WT}. If His75 plays a role for proton transfer, it could create a rate-limiting step, maybe due to ring-flip-assisted deprotonation as shown in the case of the influenza M2 proton channel.[40] On the other hand, the H75N mutation influences the kinetics of not only one but all intermediates (Table S3, Supporting Information), including the decay of the M intermediate represented by the time constant t_2. This transition is generally assigned to reprotonation of the Schiff base by the primary proton donor Glu108, which is not in direct contact with either Asp97 or His75, so the influence of the H75N mutation on the photocycle kinetics could be of indirect nature, maybe through induction of helix reorientations which could influence rate constants due to altered orientations of important side chains or through altered H^+/H_2O accessibility.

4. SUMMARY AND CONCLUSIONS

We have presented an extensive biophysical characterization of the role of His75 in green proteorhodopsin. Our solid-state NMR data show that a pH-dependent His−Asp cluster is formed via a H-bond which stabilizes the high pK_a of the primary proton acceptor Asp97 (Figure 7). Although our findings explain the molecular details of one of the key differences between proteo- and bacteriorhodopsin, it was surprising to find that His75 is not essential for proton transfer. In fact, the photocycle kinetics in PR appears to be slowed by this highly conserved residue. The existence of a similar His−Asp cluster has been shown in xanthorhodopsin,[41] where also a H-bond between ND1 of His62 and OD1 of Asp96 has been found. Such His−Asp clusters could be a general characteristic of eubacterial proton pumps. Furthermore, our solid-state NMR and optical spectroscopy data on PR_{WT} and $PR_{H75N/M}$ support and explain previous observations that PR samples close to the pK_a of Asp97 exhibit intermediate spectral and functional characteristics.

It is difficult to understand why evolution has created a protein with optimized color adaptation and a highly conserved and highly reactive residue such as His75 in its active site, which does slow its photocycle and is not needed for proton transfer. His75 does not seem to be a "structural" histidine but responds to pH changes in the environment and is therefore found as an NE2 tautomer. It is strictly conserved in hundreds of known PR variants, but not all of them may have a proton-pumping function. On the basis of the analysis of the primary sequences, microbial genomes, and further experimental results, some authors found evidence for putative "sensory" PRs which contain homologues of His75 as well.[42] Therefore, the His−Asp cluster in PR could play a role in a hypothetical sensing or regulation function of this highly abundant protein.

5. MATERIALS AND METHODS

5.1. Preparation of PR without a His-Tag. *5.1.1. Used Plasmid and Strains.* The pBAD-Topo plasmid encoding for His-tag-free PR C107S C156S C175S was kindly provided by Mark Braiman, Syracuse University, New York. The plasmid was transformed into *E. Coli* C34 (DE3).

5.1.2. Expression of PR without a His-Tag. Expression of PR without a His-tag was essentially done as described.[23] Cells were grown in a defined medium containing U-^{15}N-histidine ([^{15}N-His]PR) or U-^{13}C-histidine and 1,4-$^{13}C_2$-aspartate ([^{13}C-His-Asp]PR) with 100 μg/mL ampicillin until an OD_{600} of 0.8 was reached. For induction, a 0.5% final concentration of L-arabinose and *all-trans*-retinal (0.7 mM, dissolved in ethanol) were added. Cells were harvested by centrifugation after 3.5 h of incubation.

5.1.3. Purification. Cells were lysed in 3% *n*-octyl β-D-glucopyranoside (OG) and 1% lysozyme. After centrifugation sodium citrate (stock solution, 0.2 M, pH 5.5) was added to the supernatant in small increments to a final concentration of 150 mM. After addition of each portion, the solution was stirred for 1 h at 4 °C and then centrifuged. When the precipitated pellet became properly red, it was resuspended in 3% OG. The molar amount of PR without His-tag was determined by the absorbance of opsin-bound retinal using the extinction coefficient of 44 000 M^{-1} cm^{-1}. Purity was checked by UV/vis spectroscopy. Using this purification procedure, a ratio of A_{280nm}/A_{520nm} of 2.2 was achieved, which corresponds to a high sample purity (Figure S1, Supporting Information).

5.1.4. Reconstitution. Liposomes were prepared by lipid extrusion. We have used 1,2-dioleoyl-*sn*-glycero-3-phosphocholine (DOPC) or a

9:1 (w/w) mixture of 1,2-dimyristoyl-*sn*-glycero-3-phosphocholine/1,2-dimyristoyl-*sn*-glycero-3-phosphate (DMPC/DMPA). No differences in the NMR spectra between both preparations have been observed. For proteoliposomes, 1 mg of OG-solubilized protein (1 mg/mL) was added dropwise to 0.5 mg of liposomes and gently stirred for 30 min. To remove the detergent, 80 mg/mL biobeads (BioRad) were added stepwise. After biobead removal the PR solution was centrifuged. The pH of the protein was set at pH 9. After a final centrifugation step the reconstituted PR was transferred into a 4 mm MAS rotor.

5.1.5. pH Titration. The pH of the reconstituted samples was set with solutions containing 50 mM buffer and 5 mM MgCl. During the measurements the samples were cooled to 4 °C. Therefore, buffer solutions were set at exactly 4 °C to avoid temperature-dependent pH shifts. A list of buffers used for pH adjustment is given in the Supporting Information (Table S1).

5.2. Preparation of $PR_{H75N,M,W}$ Mutants. Mutants were prepared as described before.[10]

5.3. Solid-State NMR. All MAS NMR experiments were conducted using a 4 mm triple-resonance DVT HCN probe on Bruker wide-bore Avance III 850 and Avance 600 solid-state NMR spectrometers. The amount of PR placed in the MAS rotor was between 3 and 9 mg at a molar protein:lipid ratio of approximately 1:80. SPINAL64[43] ^{1}H decoupling (70−80 kHz) during ^{13}C and ^{15}N chemical shift evolution, acquisition (20 ms), and a 2 s recycle delay were used. All spectra were recorded from nonfrozen samples at 270 K.

5.3.1. $^{13}C-^{13}C$ PDSD. ^{13}C−^{13}C correlation experiments (Figures 2; Figure S2, Supporting Information) were carried out using proton-driven spin diffusion with 100 and 800 ms mixing times[44] on the Avance III 850 spectrometer. Shorter mixing times did not produce any cross-peaks. The spectrum was recorded with 10 kHz sample spinning with 1024 scans and 256 increments. A 1.5 ms cross-polarization contact time was applied. ^{13}C chemical shift referencing was carried out with respect to DSS (4,4-dimethyl-4-silapentane-1-sulfonic acid) through adamantane (40.49 and 31.47 ppm).

5.3.2. ^{15}N CP-MAS. Spectra (Figure 3; Figures S2 and S5, Supporting Information) were recorded on the Bruker Avance 600 at 270 K, 11.5 kHz sample spinning, and standard settings for cross-polarization and decoupling. A CP contact time of 3 ms was used. A total of 90 000 scans were accumulated per spectrum.

5.3.3. $^{1}H-^{15}N$ FSLG HETCOR (Figure 3b). The ^{15}N−^{1}H HETCOR experiments with CP magnetization transfer[45] were acquired on the Avance 600. During the proton evolution period, frequency-switched Lee−Goldburg decoupling was applied at an effective proton decoupling field of 80 kHz. A refocusing ^{15}N pulse was applied during evolution.[46] A total of 32 increments in the indirect dimension with 4K scans each were acquired. A CP contact time of 500 μs was used. The spinning speed was set to 13 kHz. The ^{1}H and ^{15}N chemical shift referencing was done via the gyromagnetic ratios through the ^{13}C chemical shift of admantane with respect to DSS. A Lee−Goldburg scaling factor of 0.57 was used for the ^{1}H chemical shifts. Different pH values were adjusted by incubating reconstituted PR samples in the buffers listed in Table S1, Supporting Information, before pelleting and transferring them into MAS rotors.

5.4. Optical Spectroscopy. *5.4.1. Vis-Pump/Vis-Probe Spectroscopy.* Transient absorption spectroscopy was performed with a setup described in ref 19. The excitation pulses were tuned to 520 nm (30 nJ pulse energy) for the PR H75N sample and to 530 nm (30 nJ pulse energy) for PR H75M. The spectral range from 430 to 750 nm was probed with single-filament white light pulses. An instrumental response function of ∼120 fs was achieved. The sample concentration was adjusted to an absorbance of ∼0.5 at the maximum of the main retinal band. The obtained data were corrected for coherent effects around time zero and for group velocity dispersion by a procedure described by Kovalenko et al.[47] For the quantitative data analysis we employed a kinetic model which describes the data as sums of exponential decays. A Marquart downhill algorithm optimizes n global time constants τ_i for all wavelengths simultaneously with wavelength-dependent amplitudes $A_i(\lambda)$ for each component. The n wavelength-dependent fit amplitudes $A_i(\lambda)$ represent the DAS for each decay component. In this definition an infinite time constant is equal to a time-independent offset in the transient absorbance changes. The measurements were performed in the following buffer solutions: (H75N) 100 mM NaCl, 0.1% OG, 10 mM MES (2-(*N*-morpholino)ethanesulfonic) acid, pH 5.6 and 7.5, or 10 mM acetate at pH 4.2; (H75M) 100 mM NaCl, 0.1% DDM (*n*-dodecyl β-D-maltoside), 10 mM MES, pH 5.6, 6.5, and 8.0.

5.4.2. Laser Flash Photolysis. The laser flash photolysis measurements were performed with a setup which is described in ref 48. The excitation pulses were adjusted to the absorption maxima of each PR sample. The repetition rate was set to 0.67 Hz. Pulse energies were approximately 2 mJ/cm^2. Transient absorbance changes at 410, 510, and 590 nm were measured repetitively (typically 1000 times) to increase the signal-to-noise ratio. The sampling frequency was set to 2.5 MHz. To cover the full time regime of PR photocycle kinetics, data points were collected up to 900 ms after excitation. To analyze the data, an exponential rate model was applied. The decay time constants were shared variables, while the pre-exponential factors (amplitudes) were fitted individually. Two different buffers were used for the measurements: 300 mM NaCl, 0.05% DDM, 20 mM MES, 20 mM TRIS, pH 7.5, for PR_{WT} and 300 mM NaCl, 0.05% DDM, 20 mM TRIS, 20 mM MES, 20 mM sodium acetate, pH 7.5, for PR_{H75N}. By direct addition of HCl or NaOH the pH of the WT protein solution was adjusted to 9, 7.5, and 5.75 or to 7.5, 5.75, and 4.5 in the case of the mutant protein solution, respectively.

5.5. BLM Experiments and Photocurrent Measurements. The experimental details were identical to those described by Friedrich and co-workers[3] (see also the Supporting Information).

■ ASSOCIATED CONTENT

Supporting Information. Further details regarding sample preparation, titration data of PR_{D227N}, additional solid-state NMR spectra (PR_{WT}, PR_{H75N}, PR_{D97N}, PR_{D227N}), analysis of time-resolved optical spectra, BLM measurements (PR_{WT}, PR_{H75N}, PR_{H75M}), and complete ref 29. This material is available free of charge via the Internet at http://pubs.acs.org.

■ AUTHOR INFORMATION

Corresponding Author
wveitl@theochem.uni-frankfurt.de; glaubitz@em.uni-frankfurt.de

■ ACKNOWLEDGMENT

We acknowledge Prof. Mark Braiman and Farhana Syed, Syracuse University, for providing a plasmid for PR without a His-tag and for an initial protocol for sample purification. We acknowledge Prof. E. Bamberg and Anja Becker, MPI Biophysics, Frankfurt, for the opportunity to carry out the BLM experiments and for helpful discussions. Dr. J. Baldus-Becker, S. J. Ullrich, and L. Reggie, Goethe University Frankfurt, are acknowledged for help with some experimental aspects of this work. This work has been funded by SFB 807 "Membrane Transport". Additional support by the Frankfurt Cluster of Excellence "Macromolecular Complexes" is acknowledged. DFG is acknowledged for an equipment grant (GL 307/2-1).

■ REFERENCES

(1) Beja, O.; Aravind, L.; Koonin, E. V.; Suzuki, M. T.; Hadd, A.; Nguyen, L. P.; Jovanovich, S. B.; Gates, C. M.; Feldman, R. A.; Spudich, J. L.; Spudich, E. N.; DeLong, E. F. *Science* **2000**, *289*, 1902–6.

(2) Sabehi, G.; Loy, A.; Jung, K. H.; Partha, R.; Spudich, J. L.; Isaacson, T.; Hirschberg, J.; Wagner, M.; Beja, O. *PLoS Biol.* **2005**, *3*, e273.
(3) Friedrich, T.; Geibel, S.; Kalmbach, R.; Chizhov, I.; Ataka, K.; Heberle, J.; Engelhard, M.; Bamberg, E. *J. Mol. Biol.* **2002**, *321*, 821–38.
(4) Rangarajan, R.; Galan, J. F.; Whited, G.; Birge, R. R. *Biochemistry* **2007**, *46*, 12679–86.
(5) Klyszejko, A. L.; Shastri, S.; Mari, S. A.; Grubmüller, H.; Müller, D. J.; Glaubitz, C. *J. Mol. Biol.* **2008**, *376*, 35–41.
(6) Shastri, S.; Vonck, J.; Pfleger, N.; Haase, W.; Kühlbrandt, W.; Glaubitz, C. *Biochim. Biophys. Acta, Biomembr.* **2007**, *1768*, 3012–9.
(7) Shi, L.; Ahmed, M. A.; Zhang, W.; Whited, G.; Brown, L. S.; Ladizhansky, V. *J. Mol. Biol.* **2009**, *386*, 1078–93.
(8) Shi, L. C.; Lake, E. M. R.; Ahmed, M. A. M.; Brown, L. S.; Ladizhansky, V. *Biochim. Biophys. Acta, Biomembr.* **2009**, *1788*, 2563–2574.
(9) Pfleger, N.; Lorch, M.; Woerner, A. C.; Shastri, S.; Glaubitz, C. *J. Biomol. NMR* **2008**, *40*, 15–21.
(10) Pfleger, N.; Woerner, A. C.; Yang, J.; Shastri, S.; Hellmich, U. A.; Aslimovska, L.; Maier, M. S. M.; Glaubitz, C. *Biochim. Biophys. Acta, Bioenerg.* **2009**, *1787*, 697–705.
(11) Walter, J. M.; Greenfield, D.; Bustamante, C.; Liphardt, J. *Proc. Natl. Acad. Sci. U.S.A.* **2007**, *104*, 2408–12.
(12) Dioumaev, A. K.; Brown, L. S.; Shih, J.; Spudich, E. N.; Spudich, J. L.; Lanyi, J. K. *Biochemistry* **2002**, *41*, 5348–58.
(13) Xiao, Y. W.; Partha, R.; Krebs, R.; Braiman, M. *J. Phys. Chem. B* **2005**, *109*, 634–641.
(14) Bergo, V.; Amsden, J. J.; Spudich, E. N.; Spudich, J. L.; Rothschild, K. J. *Biochemistry* **2004**, *43*, 9075–83.
(15) Huber, R.; Köhler, T.; Lenz, M. O.; Bamberg, E.; Kalmbach, R.; Engelhard, M.; Wachtveitl, J. *Biochemistry* **2005**, *44*, 1800–6.
(16) Imasheva, E. S.; Balashov, S. P.; Wang, J. M.; Dioumaev, A. K.; Lanyi, J. K. *Biochemistry* **2004**, *43*, 1648–55.
(17) Lenz, M. O.; Huber, R.; Schmidt, B.; Gilch, P.; Kalmbach, R.; Engelhard, M.; Wachtveitl, J. *Biophys. J.* **2006**, *91*, 255–62.
(18) Lenz, M. O.; Woerner, A. C.; Glaubitz, C.; Wachtveitl, J. *Photochem. Photobiol.* **2007**, *83*, 226–31.
(19) Neumann, K.; Verhoefen, M. K.; Weber, I.; Glaubitz, C.; Wachtveitl, J. *Biophys. J.* **2008**, *94*, 4796–807.
(20) Varo, G.; Brown, L. S.; Lakatos, M.; Lanyi, J. K. *Biophys. J.* **2003**, *84*, 1202–7.
(21) Wang, W. W.; Sineshchekov, O. A.; Spudich, E. N.; Spudich, J. L. *J. Biol. Chem.* **2003**, *278*, 33985–91.
(22) Bergo, V. B.; Sineshchekov, O. A.; Kralj, J. M.; Partha, R.; Spudich, E. N.; Rothschild, K. J.; Spudich, J. L. *J. Biol. Chem.* **2009**, *284*, 2836–43.
(23) Partha, R.; Krebs, R.; Caterino, T. L.; Braiman, M. S. *Biochim. Biophys. Acta* **2005**, *1708*, 6–12.
(24) Goux, W. J.; Allerhand, A. *J. Biol. Chem.* **1979**, *254*, 2210–2213.
(25) Sudmeier, J. L.; Bradshaw, E. M.; Haddad, K. E. C.; Day, R. M.; Thalhauser, C. J.; Bullock, P. A.; Bachovchin, W. W. *J. Am. Chem. Soc.* **2003**, *125*, 8430–8431.
(26) Bachovchin, W. W. *Magn. Reson. Chem.* **2001**, *39*, S199–S213.
(27) Sharif, S.; Schagen, D.; Toney, M. D.; Limbach, H. H. *J. Am. Chem. Soc.* **2007**, *129*, 4440–4455.
(28) Wei, Y. F.; de Dios, A. C.; McDermott, A. E. *J. Am. Chem. Soc.* **1999**, *121*, 10389–10394.
(29) Ulrich, E. L.; et al. *Nucleic Acids Res.* **2008**, *36*, D402–D408.
(30) Lakatos, M.; Lanyi, J. K.; Szakacs, J.; Varo, G. *Biophys. J.* **2003**, *84*, 3252–6.
(31) Sachs, R. K.; Halverson, K. M.; Barry, B. A. *J. Biol. Chem.* **2003**, *278*, 44222–44229.
(32) Waugh, D. S. *J. Biomol. NMR* **1996**, *8*, 184–192.
(33) Metz, G.; Siebert, F.; Engelhard, M. *Biochemistry* **1992**, *31*, 455–462.
(34) Blomberg, F.; Maurer, W.; Ruterjans, H. *J. Am. Chem. Soc.* **1977**, *99*, 8149–8159.
(35) Pacios, L. F.; Gomez, P. C.; Galvez, O. *J. Comput. Chem.* **2006**, *27*, 1650–1661.
(36) Schmidt, B.; Sobotta, C.; Heinz, B.; Laimgruber, S.; Braun, M.; Gilch, P. *Biochim. Biophys. Acta, Bioenerg.* **2005**, *1706*, 165–173.
(37) Zhong, Q.; Ruhman, S.; Ottolenghi, M.; Sheves, M.; Friedman, N.; Atkinson, G. H.; Delaney, J. K. *J. Am. Chem. Soc.* **1996**, *118*, 12828–12829.
(38) Abramczyk, H. *J. Chem. Phys.* **2004**, *120*, 11120–11132.
(39) Verhoefen, M. K.; Neumann, K.; Weber, I.; Glaubitz, C.; Wachtveitl, J. *Photochem. Photobiol.* **2009**, *85*, 540–6.
(40) Hu, F. H.; Luo, W. B.; Hong, M. *Science* **2010**, *330*, 505–508.
(41) Luecke, H.; Schobert, B.; Stagno, J.; Imasheva, E. S.; Wang, J. M.; Balashov, S. P.; Lanyi, J. K. *Proc. Natl. Acad. Sci. U.S.A.* **2008**, *105*, 16561–5.
(42) Fuhrman, J. A.; Schwalbach, M. S.; Stingl, U. *Nat. Rev. Microbiol.* **2008**, *6*, 488–94.
(43) Bennett, A. E.; Rienstra, C. M.; Auger, M.; Lakshmi, K. V.; Griffin, R. G. *J. Chem. Phys.* **1995**, *103*, 6951–6958.
(44) Szeverenyi, N. M.; Sullivan, M. J.; Maciel, G. E. *J. Magn. Reson.* **1982**, *47*, 462–475.
(45) vanRossum, B. J.; Forster, H.; deGroot, H. J. M. *J. Magn. Reson.* **1997**, *124*, 516–519.
(46) Lesage, A.; Emsley, L.; Penin, F.; Bockmann, A. *J. Am. Chem. Soc.* **2006**, *128*, 8246–8255.
(47) Kovalenko, S. A.; Dobryakov, A. L.; Ruthmann, J.; Ernsting, N. P. *Phys. Rev. A* **1999**, *59*, 2369–2384.
(48) Verhoefen, M. K.; Bamann, C.; Blöcher, R.; Förster, U.; Bamberg, E.; Wachtveitl, J. *ChemPhysChem* **2010**, *11*, 3113–3122.